Applied Catalysis B: Environmental 244 (2019) 494–501

Contents lists available at ScienceDirect

Applied Catalysis B: Environmental

journal homepage: www.elsevier.com/locate/apcatb

Highly active and stable ruthenate pyrochlore for enhanced oxygen evolution reaction in acidic medium electrolysis

Qi Feng[a,b], Qi Wang[b], Zhen Zhang[a,b], Yongyueheng Xiong[b], Hanyi Li[b], Yao Yao[b], Xiao-Zi Yuan[c], Mark C. Williams[d,1], Meng Gu[b], Hong Chen[b], Hui Li[b,*], Haijiang Wang[d,*]

[a] School of Materials Science and Engineering, Harbin Institute of Technology, Harbin 150001, China
[b] Department of Materials Science and Engineering, Southern University of Science and Technology, Shenzhen 518055, Guangdong, China
[c] Research Center of Energy, Mining and Environment, National Research Council Canada, 4250 Wesbrook Mall, V6T1W5, Canada
[d] Department of Mechanical and Energy Engineering, Southern University of Science and Technology, Shenzhen, 518055, China

ARTICLE INFO

Keywords:
Oxygen evolution reaction
Electrocatalyst
Water electrolysis
Pyrochlore oxides
Acid media

ABSTRACT

Developing active, acid-stable and cost-effective electrocatalysts for oxygen evolution reaction (OER) is a primary challenge to directly produce hydrogen from water electrolysis. IrO_2 is the best-known catalyst in acid medium due to its good activity and stability, but it's too expensive to be used in large amounts. To overcome this economical constraint, the use of low amount of iridium electrocatalyst is required. Recently, ruthenium pyrochlore oxides ($A_2Ru_2O_{7-}\delta$) as OER catalysts have drawn extensive interests due to reduced content of precious metal relative to RuO_2 or IrO_2, though their OER catalytic activity still needs to be further improved. In this work, we, for the first time, developed a highly active and stable $Y_{1.85}Zn_{0.15}Ru_2O_{7-}\delta$ electrocatalyst, the A site doped yttrium ruthenate pyrochlore for OER. The mechanism of A site doped ruthenate pyrochlore improving OER performance is revealed. The partial substitution of Y^{3+} ions by smaller Zn^{2+} leads to a formation of oxygen vacancies and mixed valences of Ru (Ru^{4+} and Ru^{5+}), which, in turn, significantly alter the electronic properties and thus the electrocatalytic activity and electrical conductivity of the developed electrocatalyst for OER. The $Y_{1.85}Zn_{0.15}Ru_2O_{7-}\delta$/acetylene black (AB) electrocatalyst exhibits sevenfold higher activity than the IrO_2/AB reference catalyst; twofold higher activity than $Y_2Ru_2O_{7-}\delta$/AB, with a Tafel slope of 36.9 mV dec^{-1}; and higher stability than IrO_2/AB in acidic media. Using a home-made proton exchange membrane electrolyser device, a high cell performance is achieved at 25 °C with an electrolysis current density of 0.46 A cm^{-2}, confirming a promising prospect of $Y_{1.85}Zn_{0.15}Ru_2O_7-\delta$ electrocatalyst for practical water electrolysis applications.

1. Introduction

With a growing market of electricity generation from intermittent renewable energy sources, energy storage has become more and more important [1]. Hydrogen production through water electrolysis is an effective solution for energy storage. The high current density, low gas permeability, small mass-volume characteristic and rapid dynamic response of proton exchange membrane water electrolysers (PEMWEs) make them the most promising devices for hydrogen production [2,3]. However, harsh corrosive conditions and high anodic overpotentials in PEMWEs require high activity and durability for anode materials [4]. Feasible catalysts used in such conditions are mainly limited to precious metal oxides, such as IrO_2, and RuO_2. Both RuO_2 and IrO_2 show a metallic behavior with a relatively high electrical conductivity of 10^4 $cm^{-1}\Omega^{-1}$ [5].

RuO_2 is presently the most active electrocatalyst for OER in acid medium; however, it is easy to be oxidized to soluble RuO_4 under anodic potentials [6]. IrO_2 is the best known catalyst in acid medium due to its good activity and stability, but it is much more costly than RuO_2 [7]. Iridium is one of the scarcest elements in the earth with the abundance 10 times lower than Pt [4]. The price of Iridium is as high as 500 $ per oz., about 12 times higher than Ru (42 $ per oz.) [8]. Since Ru is more economical than Ir, researchers always attempt to stabilize RuO_x against corrosion/dissolution [4,9–11]. As such, other earth abundant elements are introduced into Ru-based oxides to reduce the corrosion rate of Ru [10–13]. It has been proved that the stability of RuO_2 can be greatly improved by mixing with IrO_2 [3,14–16]. However, the noble metal content in these electrocatalysts is still too high,

* Corresponding authors.
E-mail addresses: hui.li@sustc.edu.cn (H. Li), wanghj@sustc.edu.cn (H. Wang).
[1] Fellow of the Electrochemical Society.

https://doi.org/10.1016/j.apcatb.2018.11.071
Received 24 July 2018; Received in revised form 16 November 2018; Accepted 24 November 2018
Available online 26 November 2018

impeding cost reduction. Some researchers have attempted to use stable support materials so as to lower the noble metal content in OER electrocatalysts [7,17]. Unfortunately, most of the supports exhibit very poor electronic conductivity, hampering the charge transport kinetics [18]. Another feasible approach is the preparation of complex oxides based on precious metals. Such catalysts are strategically designed to obtain a favorable balance among the activity, stability and cost [1].

Pyrochlore is a complex oxide with a general formula of $A_2B_2O_{7-y}$, where A is typically Pb, Bi, Tl, or Ln (rare-earth metal); and B can be Ir, Ru, or Nb. Among them, iridium pyrochlore and ruthenium pyrochlore were found to remain active and stable for OER in water electrolysis [1,19–22]. There are rich oxygen defects in such complex oxides which can enhance OER activity [21,23,24]. Ir-free catalysts for OER are more favorable due to their lower cost. As such, $Y_2Ru_2O_{7-\delta}$ (YRO) was recently discovered to significantly enhance the cell performance over conventional RuO_2 electrocatalysts with respect to OER activity and stability in acidic medium [19,21]. Because of the n-type semiconducting property, YRO possesses a low electrical conductivity, resulting in a high Ohmic loss [25–28]. Doping of suitable foreign elements in either or both of the A and B sites ($A_2B_2O_{7-\delta}$) provides opportunities for further modifying material properties, including the improvement of electrical conductivity [27,29,30] and oxygen vacancies. It has been reported that the electrical conductivity of $Y_{1.85}Zn_{0.15}Ru_2O_{7-\delta}$ (YZRO) is enhanced by two orders of magnitude compared to YRO at room temperature [30]. By substituting in the A-site, the catalytic activity can also be greatly enhanced by tuning the electronic properties and the interface binding strength.

In this context, we report an A site doping of YZRO electrocatalysts with highly active and stable properties towards OER in strong acid medium. The electrochemical activity is firstly evaluated by traditional three-electrode testing system. YZRO/AB electrocatalysts shows low overpotential and small Tafel slope to drive OER process. The OER overpotentials of YZRO/AB and YRO/AB are, respectively, 290 mV and 307 mV at 10 mA cm^{-2}, while the overpotential of IrO_2/AB at 10 mA cm^{-2} is 340 mV as measured. The Tafel slopes for YZRO/AB and YRO/AB are 36.9 mV dec^{-1} and 40.8 mV dec^{-1}, respectively, which are both lower than that of IrO_2/AB with a value of 43.2 mV dec^{-1}. It is important to highlight that YZRO/AB has a much better stability than IrO_2/AB. Furthermore, the activity of YZRO/AB electrocatalysts is also examined in a home-made PEM electrolyzer using the as-prepared YZRO/AB and commercial Pt/C as anode catalyst and cathode catalyst, respectively. For a single cell tests, a high current density of 0.46 A cm^{-2} is achieved under an applied voltage of 1.7 V at 25 °C.

2. Experimental

2.1. Material preparation

YZRO was synthesized with modifications to previously described methods by Kim et al. [19]. $Y(NO_3)_3{\cdot}6H_2O$ (99.9%, Macklin), $RuCl_3$ (Macklin), $Zn(CH_3COO)_2{\cdot}2H_2O$ (Macklin, 98%) and citric acid (99%, Macklin) were used with no further purification. 177 mg of $Y(NO_3)_3{\cdot}6H_2O$, 103.7 mg $RuCl_3$, and 8.2 mg $Zn(CH_3COO)_2{\cdot}2H_2O$ were dissolved in deionized water (18.2 MΩ-cm resistivity, Ulupure) with stirring. Next, 420.3 mg of citric acid were added into the mixed solution. Then, the solution was heated in a water bath with continuous stirring at 85 °C. Residual water was removed in the vacuum oven (~30 mbar) at 110 °C for overnight. Before the precursor was transferred into a porcelain crucible for heat treatment, the powder was ground for about 15 min. The powder was heated up to 600 °C at a rate of 5 °C min^{-1} for 6 h, followed by 1050 °C at a rate of 5 °C min^{-1} for 12 h. The YRO powder as one of the reference catalysts was analogously synthesized. The commercial IrO_2 (99.9%, Sunlaite) was also used as reference catalyst.

2.2. Material characterization

X-ray diffraction (XRD) pattern was recorded in a Bruker D8 Advance ECO (Cu Kα, λ = 1.5046 Å, 40 kV and 25 mA) from 10° to 90° to investigate the crystalline structure of the powder. For the sake of characterizing the morphology of nanoparticles, scanning electron microscopy (SEM, TESCAN VEGA 3 LMH, acceleration voltage set at 10 kV) was carried out. To further clarify the crystal phase of pyrochlore oxides, high-resolution transmission electron microscopy (HRTEM) was performed in double Cs-corrected TEM Titan Themis with an operating voltage of 300 kV. High-angle annular dark field of scanning TEM (STEM-HAADF) was conducted to investigate the cross section of the pyrochlore catalyst. Energy-dispersive spectroscopy (EDS) mapping was also carried out to confirm the elements of the particles. XPS measurement was applied to analyze surface species and chemical states of the samples, using a PHI 5000 VersaProbe II (Japan) with a monochromatic Al Kα (hυ = 1486.69 eV) X-ray source. The main line of C 1s spectrum (adventitious carbon) was used as the corrected line, which was set to 284.8 eV.

The electrical conductivity of YZRO, YRO and IrO_2 was measured using a Soochow Jingge ST2253 digital tester via the standard DC four probe modality. Firstly, 0.8 g of the YZRO, YRO and IrO_2 were weighed, respectively, by an electronic balance. Then, disc-shaped samples with a radius of 6 mm were obtained by cold isostatic pressing (180 s) of the powder at 8 MPa followed by sintering in air at 1000 °C for 18 h to achieve proper density of the samples.

2.3. Electrode preparation and electrochemical measurements

Acetylene black (Hesen, Shanghai, AB) was used as the support for these catalysts. AB plays a role of dispersant and an electronic conductor during the electrochemical experiments. In a typical procedure, catalyst inks were prepared to make thin film rotating disk electrodes (RDEs) using 5 mg metal oxides, 1 mg acetylene black, 0.2 mL of deionized water, 0.8 mL of isopropyl alcohol (IPA) and 30 μL of 5 wt.% Nafion solution (Dupont). Then the mixture solution was sonicated for 2 h in an ice bath to generate a homogeneous ink. The thin film RDE was finally obtained by pipetting 8 μL of the catalyst ink onto the glassy carbon electrode with a diameter of 5 mm.

Electrochemical measurements were conducted in a three-electrode cell containing 0.5 M H_2SO_4 solution with an RDE setup (Pine Instruments, USA) and a Solartron analytical Cell Test system (1470E/1400). The three-electrode cell consists of the hydrogen reference electrode, the catalyst loaded glassy carbon working electrode, and the platinum net (1 × 1 cm^2) counter electrode.

Polarization curves were run between 1.1 and 1.65 V at a scan rate of 10 mV s^{-1} under a rotating speed of 1600 rpm. Electrochemical impedance measurements (EIS) were performed in a potentiostatic mode with an amplitude of 10 mV over a frequency range of 100,000 – 0.1 Hz. To investigate the stability, cyclic voltammetry (CV) measurements were scanned from 1.35 to 1.6 V at a rate of 100 mV s^{-1}. Chronopotentiometry tests were also performed with a constant current. All potentials are referenced to the reversible hydrogen electrode (RHE), unless otherwise claimed.

2.4. Preparation of MEA and single cell test

YZRO or commercial IrO_2 (Sunlaite) mixed with AB (mass ratio, 5:1) was used as the anode of the catalyst coated membrane (CCM), while Pt/C (47.7 wt.%, Tanaka®) was used as the cathode of the CCM with Nafion® membrane (N212, 50 μm thick) sandwiched in the middle as the solid polymer electrolyte. Detailed procedures are as follows. The catalyst powders were weighed accurately and then placed into a beaker. An appropriate amount of deionized water was firstly poured into the beaker. IPA was then added dropwise with the same volume as the deionized water, followed by an addition of Nafion ionomer. The

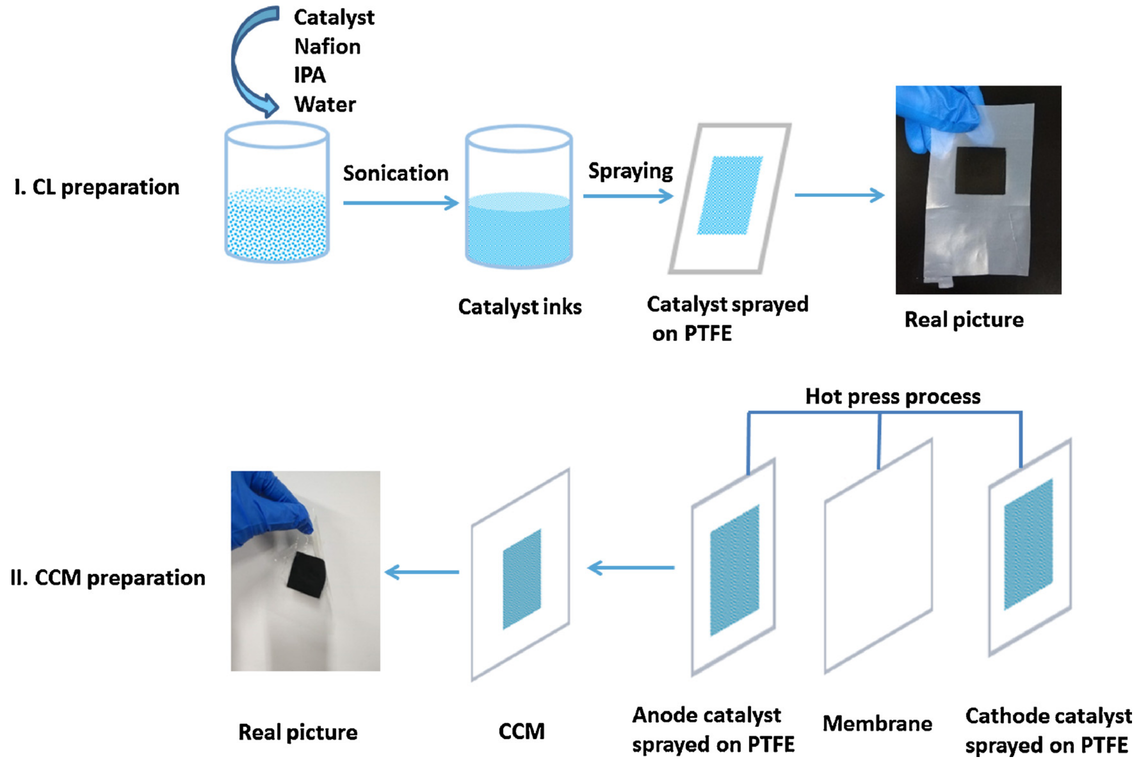

Fig. 1. Diagrammatic drawings of the process for CL preparation and CCM preparation.

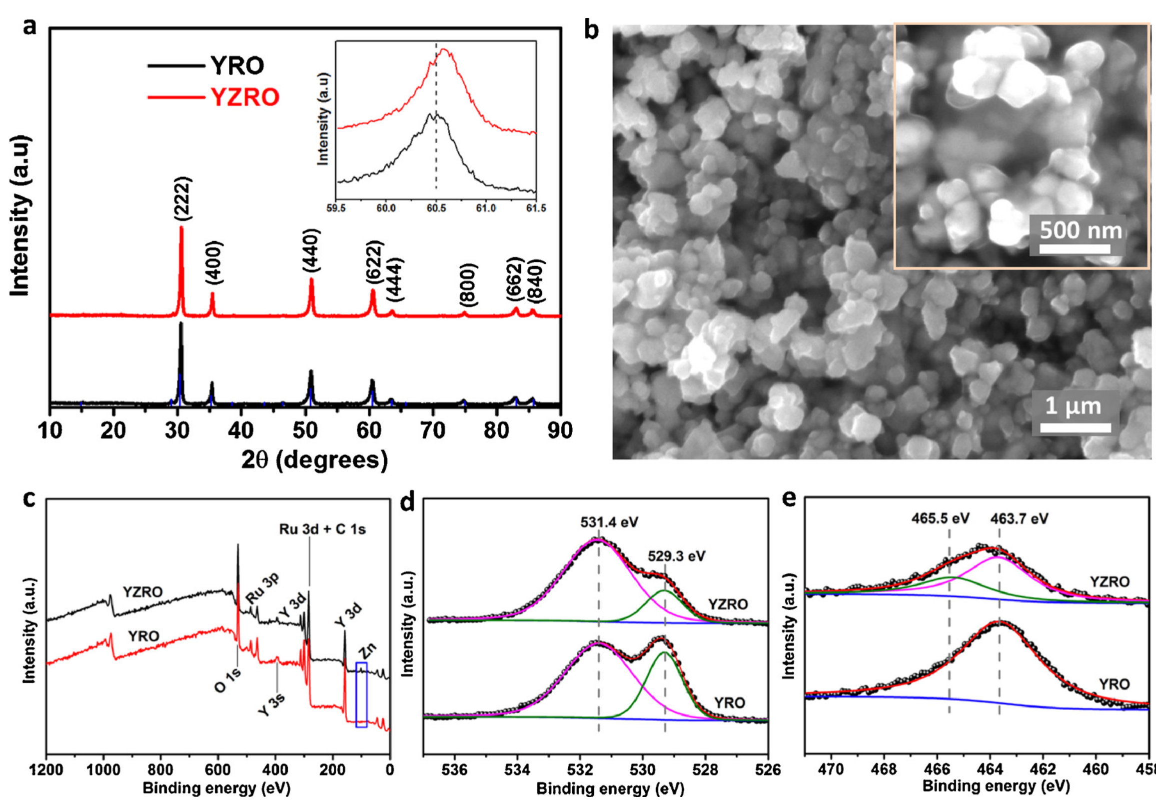

Fig. 2. (a) XRD patterns of the YRO and YZRO powders. (b) SEM image of YRZO with the inset magnifying the local region. (c) A full XPS survey of YRO and YZRO. (d) High-resolution XPS spectra of O 1 s for YRO and YZRO. (e) High-resolution XPS spectra of Ru $3p_{3/2}$ for YRO and YZRO.

Nafion ionomer contents of the anode catalyst layer and the cathode catalyst layer were determined to be 15 and 25 wt.%, respectively. A homogeneous suspension was obtained after sonication for 2 h. In general, several methods can be used to coat catalyst layers on the proton exchange membrane [4,31–33], such as blade coating, screen printing and spray coating. For small area CCM preparation, spray coating method is usually more preferred due to its economic superiority.

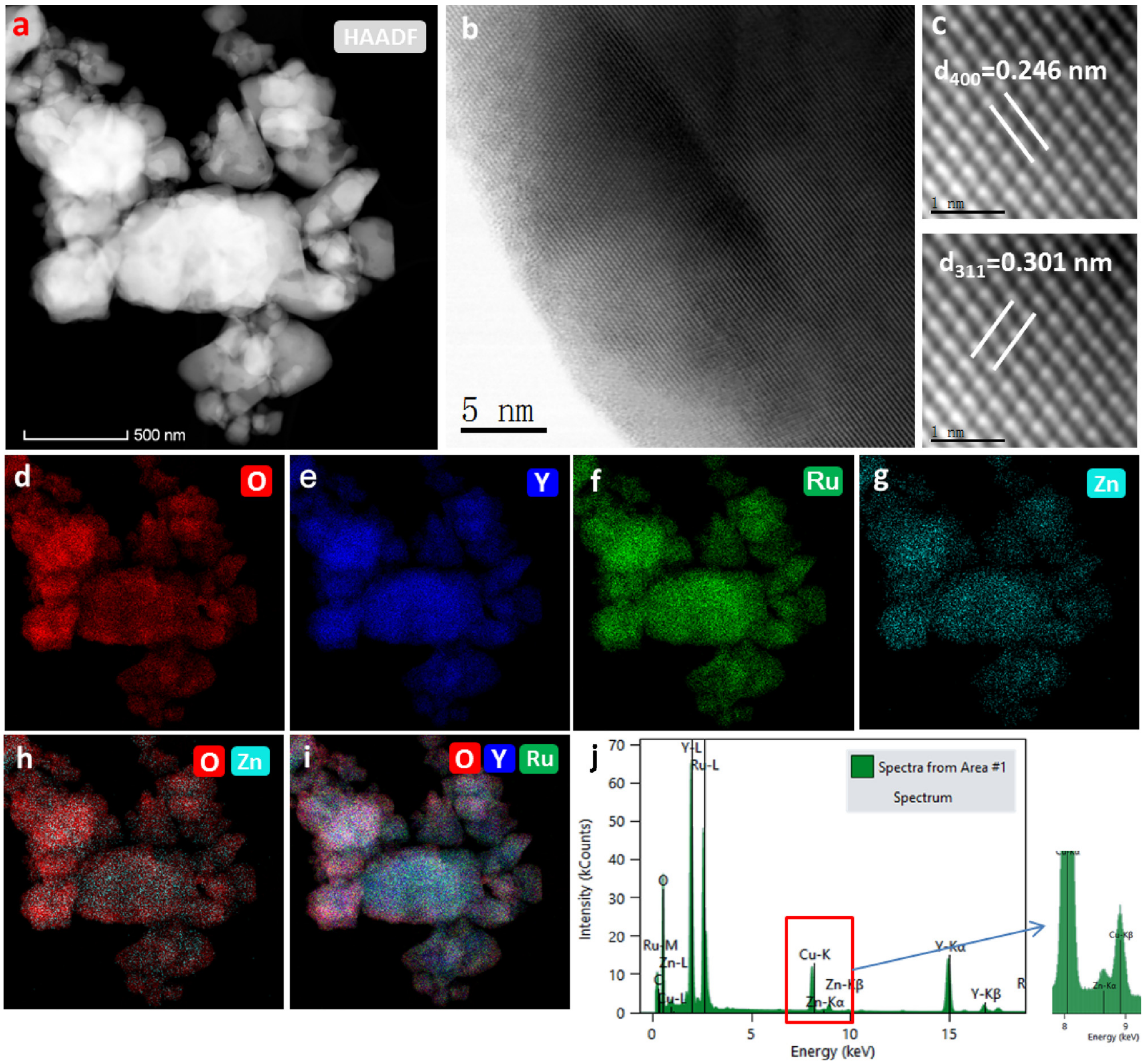

Fig. 3. (a–b) HRTEM images of the YRZO nanoparticles at (a) low and (b) high magnifications. (c) HRTEM image of the YRZO nanoparticles with the d spacing of (400) and (311) planes. (d–i) separate and overlapped EDS mapping images of O, Y, Ru, Zn in the YRZO nanoparticles. (j) EDS profiles of the YRZO nanoparticles.

Preparation of CCMs is illustrated in Fig. 1. Catalytic suspensions (inks of catalyst powder and Nafion ionomer in solvents) were sprayed onto thin and flat PTFE sheets (0.1 mm). For the anode catalyst layer (CL), the loading of YZRO/AB was 3 mg cm^{-2}, whereas the loading of IrO_2 was 2.5 mg cm^{-2} for comparison. For the cathode CL, the loading of Pt was 1.5 mg cm^{-2}. The Nafion membrane (N212) was then sandwiched between the two catalyst coated PTFE sheets. By hot pressing at 30 kg cm^{-2} and 135 °C for 3 min, the CLs were transferred to the membrane with an active area of 2 cm^2. The resulting CCM was placed between two sheets of carbon paper as gas diffusion layers (GDL) to form the membrane electrode assembly (MEA). Finally, the as-prepared MEA was assembled with two titanium bipolar plates, silicon gaskets and aluminum alloy end plates using a torque of 3.5 N. Deionized water was supplied by a peristaltic pump. Polarization curves were measured by recording the current density while changing the cell voltage from 1.1 to 1.8 V with a scan rate of 10 mV s^{-1}. The EIS was carried out with an amplitude of 10 mV in a frequency range from 100,000 Hz to 0.2 Hz.

3. Result and discussion

Fig. 2a shows the XRD patterns of YZRO and YRO. Other components of $Y_{2-x}Zn_xRu_2O_7$ (x = 0 ~ 0.3) are shown in Fig. S1. Notably, all diffraction peaks of the un-doped and doped powders match well with the pyrochlore cubic phase (Fd3m), suggesting the complete incorporation of Zn into the lattice of YZRO. As a result of the substitution of Y^{3+} ions by smaller Zn^{2+} ions in the host lattice, as shown in the inset of Fig. 2a, the peak of YZRO at 60.5° (622 crystal plane) shifts towards higher diffraction angles in the XRD pattern [29,30]. Fig. 2b exhibits the aggregated YZRO particles consisting of granular submicron-sized particles (see the inset of Fig. 2b). The SEM micrograph combined with the EDS mapping of the YZRO elements clearly shows the presence of Y, Zn, Ru and O (Fig. S2 and S3).

Fig. 2c presents the full XPS spectra for the doped and undoped pyrochlores. The core composition of Y, Ru and O can be confirmed in the overview of a full XPS scan. The regional high-resolution XPS spectra of Zn at a binding energy (BE) of 1022 eV in the Zn doped YZRO sample (Fig. S4), further evidence that Zn atoms are doped into the YRO

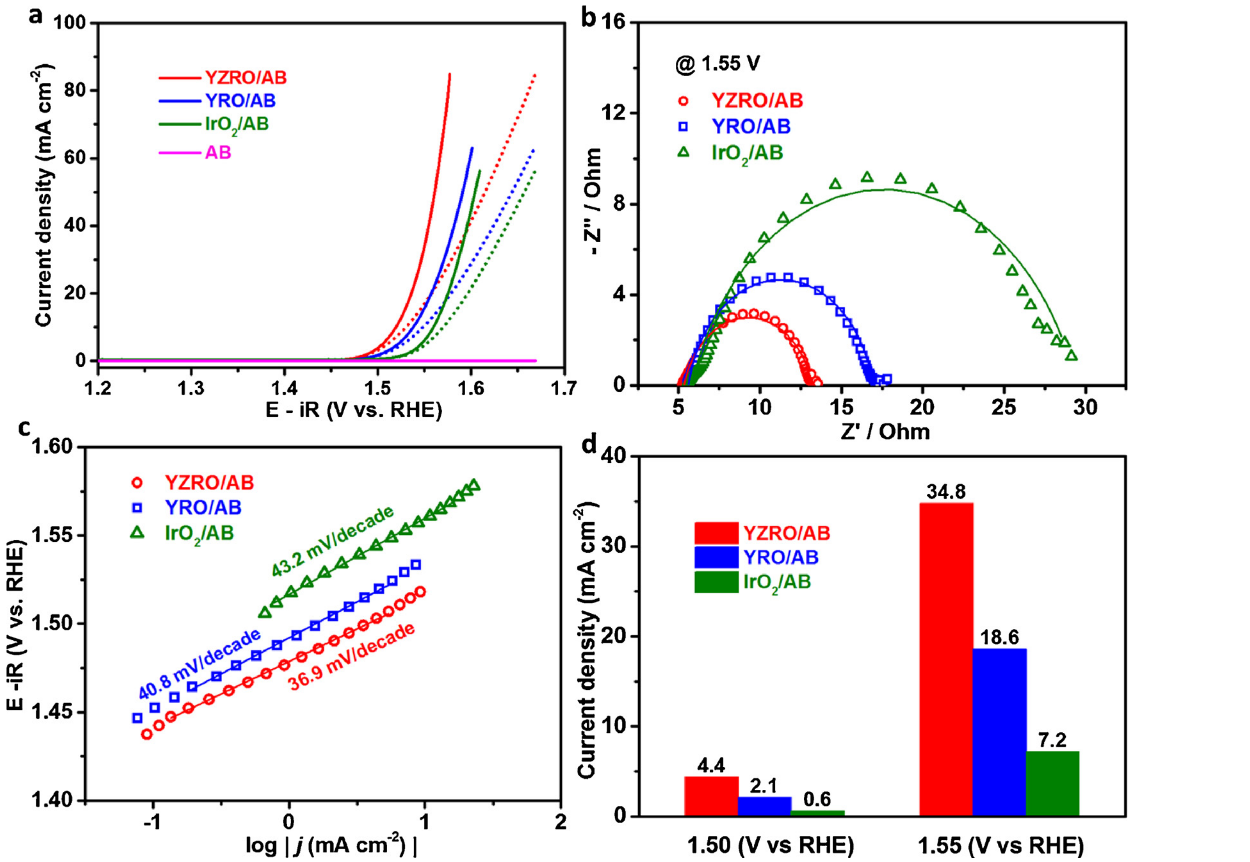

Fig. 4. (a) Polarization curves for the YZRO/AB electrocatalyst, and the reference electrocatalysts of YRO/AB, IrO_2/AB and AB, the short dot curve is the raw data without iR compensation. (b) Comparison of current densities obtained at 1.50 V and 1.55 V for YZRO/AB, YRO/AB and IrO_2/AB. (c) Tafel plots derived from (a). (d) Nyquist plots of the YZRO/AB, YRO/AB and IrO_2/AB electrocatalysts at 1.55 V. The solid curves are the fitted data.

lattice. Fig. 2d–e show the regional XPS of O 1s and Ru $3p_{3/2}$ for the two pyrochlores. Note that the integral background of the spectra and deconvolutions is deducted. As shown in Fig. 2d, the O 1 s spectra can be well fitted into two peaks, corresponding to 529.3 and 531.4 eV, ascribed to the surface lattice oxygen (O_{latt}) and the adsorbed oxygen (O_{ads}, viz., O^{2-}, $O_2{}^{2-}$, O^-, OH^-) [34–37], respectively. It is obvious that the intensity of the O_{latt} peak decreases in YZRO, indicating a partial removal of O_{latt} due to the Zn doping in the lattice of YRO. As a result, the spectrum of YZRO exhibits a greater O_{ads} peak area (79.9%) than YRO (68.5%), indicating higher oxygen vacancies which are usually recognized as the active sites for the OER electrocatalysis process [35,38]. Actually, it has been reported that A site of pyrochlores doped with 2+ cation can give rise to the hole effect [39,40]. Subsequently, the number of oxygen vacancies of the doped pyrochlores greatly increases [39,40]. As shown in Fig. 2e, the peak of the undoped sample (YRO) can be fitted by a BE of 463.6 eV, which is in accordance with the 4+ valence for Ru [30,41]. However, the Ru $3p_{3/2}$ spectra of the doped sample (YZRO) can be fitted with two corresponding peaks centered at 463.6 and 465.5 eV. The peak at 465.5 eV is ascribed to Ru^{5+}, which is consistent with the result reported [30,41]. From the XPS results, we can conclude that Zn doped $Y_2Ru_2O_7$ leads to a formation of oxygen vacancies and mixed valences of Ru (Ru^{4+} and Ru^{5+}), which, in turn, significantly alter the electronic structure and thus the electrocatalytic activity and electrical conductivity of $Y_2Ru_2O_7$ for OER.

Fig. 3a–c show the STEM-HAADF images of the YZRO nanoparticles. As can be seen, the doped YZRO is composed of highly pure and crystalline nanoparticles with a pyrochlore oxide structure. The interlayer d–spacing of (400) and (311) crystal planes of the pyrochlore, shown in Fig. 3c, are 0.246 and 0.301 nm, respectively. The HRTEM images of the undoped YRO pyrochlore are shown in Fig. S5. Obviously, the lattice fringe spacing of YRO is smaller after Zn doping, in agreement with the shift of the XRD peak. Based on observations from the EDS map-scans, it is confirmed that YZRO is successfully synthesized with a homogeneous distribution of Y, Ru, O and Zn, as shown in Fig. 3d–i.

3.1. Electrochemical activity studies

The OER activities of all samples were evaluated and compared using the same electrochemical analysis under the same conditions. The polarization curves were corrected with iR-compensation. The compensated ohmic resistance of YZRO/AB, YRO/AB and IrO_2/AB in 0.5 M H_2SO_4 are 5.2, 5.5 and 5.5 Ω, respectively, as shown in Fig. S6. The onset potential of the YZRO/AB electrocatalyst exhibits the lowest among the series. Higher OER activity is achieved for the YZRO/AB electrocatalyst (overpotential, η = 0.291 V at 10 mA cm^{-2}) than the reference electrocatalyst of YRO/AB (η = 0.308 V) and IrO_2/AB (η = 0.329 V). Based on the RDE tests, as shown in Fig. 4b, the current density of YZRO/AB is 4.4 mA·cm^{-2} at 1.50 V. This value is over sevenfold higher than that of the IrO_2/AB reference catalyst (0.6 mA cm^{-2}), and twofold higher than that of YRO/AB. Obviously, YZRO/AB greatly promotes the OER activity in acidic media. The electrochemical performance of other components of $Y_{2-x}Zn_xRu_2O_7$/AB (x = 0 ~ 0.3) are shown in Fig. S7.

The OER kinetics on all electrodes is compared via Tafel plots (Fig. 4c). Among the series, YZRO/AB exhibits the lowest Tafel slopes of only 36.9 mV dec^{-1}, in comparison with 40.8 mV dec^{-1} for YRO/AB and 43.2 mV dec^{-1} for IrO_2/AB. This indicates that the OER kinetics is largely enhanced on the YZRO/AB electrode. The Tafel slopes for YRO/AB and IrO_2/AB electrocatalysts are in good accordance with the

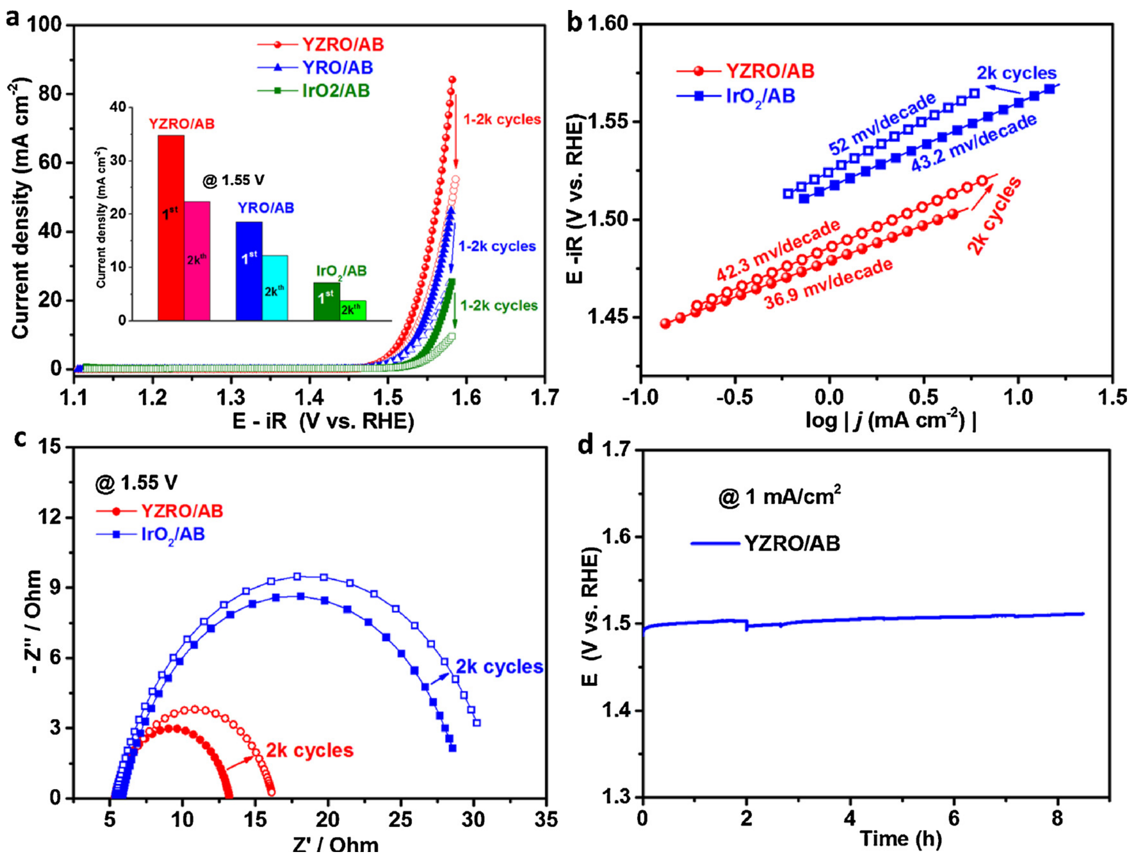

Fig. 5. (a) Polarization curves before and after 2000 CV cycles. The inset compares the current density for the YZRO/AB, YRO/AB and IrO_2/AB electrocatalysts at 1.55 V versus RHE. (b) Chronopotentiometry performance at 1 mA cm^{-2} for 8.5 h. (c) Tafel plot before and after 2000 CV cycles. (d) Nyquist plots of YZRO/AB and the reference IrO_2/AB catalyst before and after 2000 CV cycles.

previously reported values [19,20,42–44]. In the past years, OER mechanisms based on density functional theory (DFT) calculations [45,46] and OER kinetics [47] have been extensively studied. At present, one of generally accepted OER mechanism in an acidic solution is the so called “Electrochemical Oxide Path” [48], shown as follows:

$$S+ H_2O \rightarrow S- OH_{ads} + H^+ + e^- \quad (1)$$

$$S- OH_{ads} \rightarrow S-O_{ads} + H^+ + e^- \quad (2)$$

$$2\,S- O_{ads} \rightarrow 2S + O_2 \quad (3)$$

This Electrochemical Oxide Path starts with a charge-transfer process to form an adsorbed hydroxyl species onto the surface of the active site S. Subsequently, a second charge transfer process is generated to deprotonate the adsorbent followed by a third step to form an oxygen molecule and the back formation of two active sites [49]. Obviously, according to the “Electrochemical Oxide Path” mechanism, improving the electrical conductivity of the catalyst can benefit the first and second charge-transfer processes. As shown in Table S1, the electrical conductivity of YZRO (0.27 S m^{-1}) is 251 times higher than YRO (1.1×10^{-3} S m^{-1}). The enhancement of electrical conductivity of YZRO can definitely facilitate the charge transfer process. Apparently, the electrical conductivity of YZRO is much lower than IrO_2 (1.6×10^4 S m^{-1}). Fig. S8 demonstrates the OER performance of pure catalyst (YZRO, YRO and IrO_2). Without the addition of carbon support, YZRO catalyst shows a relatively low OER performance compared to IrO_2 due to its larger particle sizes (Fig. S9), lower specific surface area (Fig. S10) and less electrical conductivity than IrO_2.

As OER electrocatalysts, ruthenate and iridate pyrochlores, including $Bi_2M_2O_7$ and $Pb_2M_2O_7$ (M = Ru or Ir), have been investigated. The most detailed reaction mechanism for such materials is the one proposed by Goodenough et al. [20,22]. They indicate that the active site on $Pb_2Ru_2O_7-\delta$ for OER is a surface O^- species, which is stabilized by the oxidation of a surface cation with a redox couple Ru^{5+}/Ru^{4+} lying close to the top of the O^{2-}:$2p^6$ valence band. In the YZRO compounds which contain partial 5+ valences for Ru at oxidizing potentials, the equilibrium of reaction, $Ru^{5+}O^{2-} \leftrightarrow Ru^{4+}O^-$, is likely to be biased to the right. Hence, more active sites for OER generate in this situation [50,51]. This explanation is in good agreement with the XPS results discussed above. Additionally, it was also reported that the multiple Ir sites could contribute to the redox activity [52] and surface reactivity [53] during OER. Aricò et al. [13] investigated the effect of Ir oxidation state on the performance of OER catalysts in PEMWE. They concluded that a high oxidation of IrO_2 was more beneficial to decrease OER overpotential. Ru probably also has such features due to its similar chemical properties of Ir.

During OER, the catalytic performance was examined by EIS and analyzed using an equivalent electrical circuit, consisting of the charge transfer resistance (R_{ct}), the solution resistance (R_{sol}), and the double layer capacitance (C_{dl}) [19]. As shown in the Nyquist plots (Fig. 4d), the semicircle of YZRO/AB is much smaller at an applied potential of 1.55 V compared with those of the YRO/AB and IrO_2/AB electrodes. The charge transfer resistance is 7.9 Ω for the YZRO/AB electrocatalyst, much lower than that of YRO/AB (11.3 Ω) and IrO_2/AB (23.7 Ω). This clearly indicates that YZRO/AB is more active towards OER due to a faster charge transfer process than the YRO/AB and IrO_2/AB reference catalysts.

3.2. Electrochemical stability studies

The electrochemical stability of the metal oxides was evaluated by cyclic voltammogram (CV) and chronopotentiometric (CP) electrolysis in a manner similar to the approach reported by Kim et al. [19].

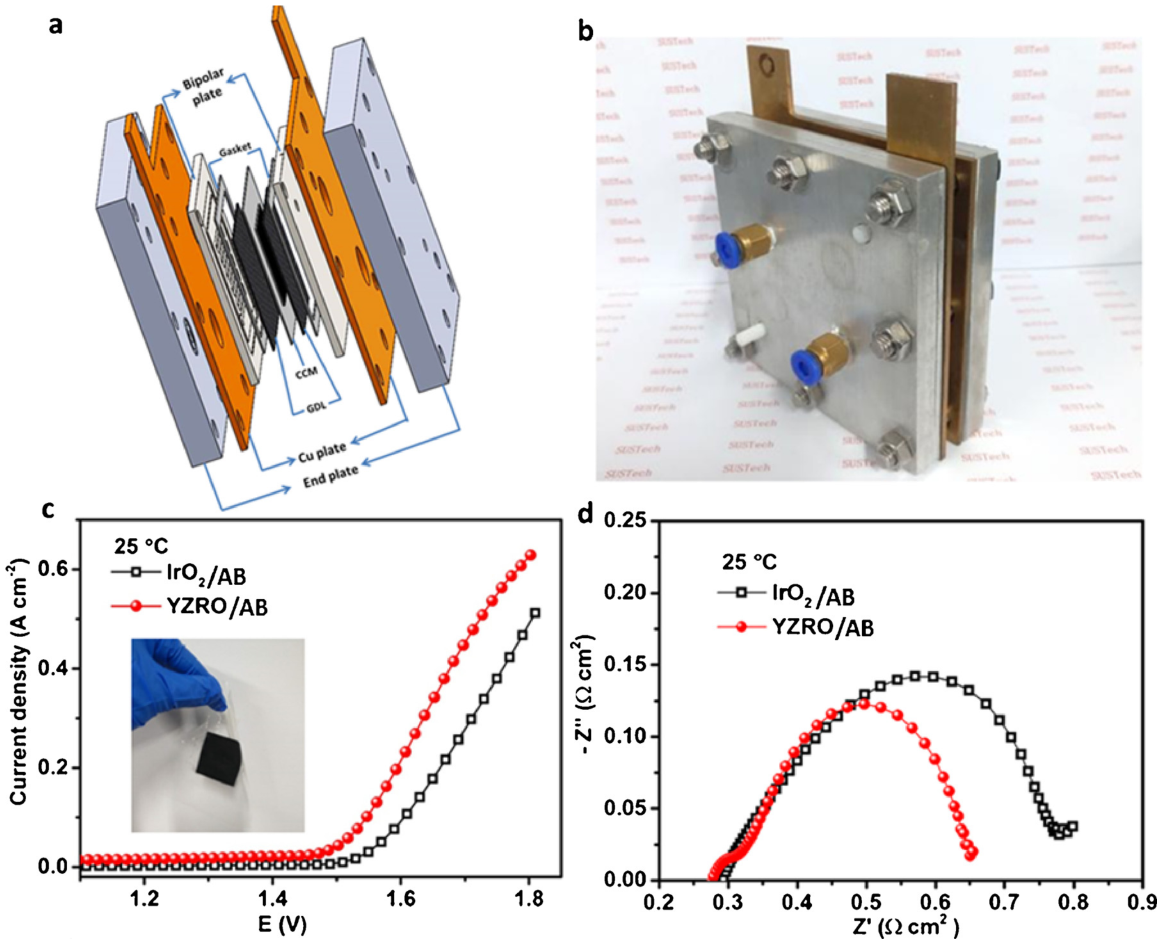

Fig. 6. (a) Schematic illustration and (b) a photo of the PEM electrolyzer device. (c) Polarization curves for the PEM electrolyser with YZRO/AB and IrO_2/AB as the anode catalysts, respectively, at 25 °C. The inset shows the as-prepared CCM. (d) Electrochemical impedance spectra (EIS) with a cell voltage of 1.55 V at 25 °C.

Stability tests were performed for 2000 CV cycles from 1.35 V to 1.6 V and the polarization curves were compared before and after the stability measurements. Fig. 5a shows the OER polarization curves for the YZRO/AB, YRO/AB and IrO_2/AB electrocatalysts before and after 2000 CV cycles. At 1.55 V, the current density of the YZRO/AB electrocatalyst decreases by 35.6% (from 34.8 mA cm^{-2} to 22.4 mA cm^{-2}) after 2000 cycles, whereas the current densities of the YRO/AB (from 18.6 mA cm^{-2} to 12.3 mA cm^{-2}) and IrO_2/AB (from 7.2 mA cm^{-2} to 3.8 mA cm^{-2}) electrocatalysts decrease by 33.9% and 47.6%, respectively. This indicates that partial Zn substitutes for Y at A sites ($A_2B_2O_{7-}\delta$) does not influence the intrinsic stability of YRO. The high structural stability of YRO can be ascribed to rigid RuO_6 structure [21].

Fig. 5b shows the Tafel slopes before and after 2000 CV cycles for all the samples. After 2000 CV cycles, all the Tafel slopes increase. For YZRO/AB, the Tafel slope increases from 36.9 mV dec^{-1} to 42.3 mV dec^{-1}, while from 43.2 mV dec^{-1} to 52.0 mV dec^{-1} for IrO_2/AB, and from 40.8 mV dec^{-1} to 45.8 mV dec^{-1} (Fig. S11) for YRO/AB. Fig. 5c presents the Nyquist plots of YZRO/AB and IrO_2/AB. As can be seen, the charge transfer resistances of YZRO/AB and IrO_2/AB both increase as well after 2000 CV cycles. By applying a current density of 1.0 mA cm^{-2} for 8 h and observing the potential change, shown in Fig. 5d, it is found that YZRO/AB remains stable for the entire test (the experiment was interrupted at the bluff in Fig. 5d). In addition, the stability test was also conducted at a higher current density of 10 mA cm^{-2}. As shown in Fig. S12, the potential (vs RHE) retained quite stable for the whole test. To verify the structure information of the catalyst, TEM images and the corresponding HRTEM profiles of the YZRO/AB electrocatalysts were examined before and after CP measurements. As can be seen in Fig. S13 and Fig. S14, the HRTEM images reveal that a crystalized cubic structure is well kept for the YZRO/AB electrocatalysts after the CP test. The EDS mapping, shown in Fig. S14, also indicates that the compositions of YZRO/AB (Y, Ru, Zn, O) have no obvious change, suggesting that the catalyst has a high stability even under a relatively harsh OER condition.

3.3. MEA and single cell tests

To further evaluate the activity of the as-prepared YZRO electrocatalyst for OER, cell test was conducted using a home-made electrolysis device. The electrolyzer cell design used in this study is presented in Fig. 6a. The cell consists of aluminum end plates, silicon gaskets, current collectors, MEA, and GDL. The cell is compressed by 8 M6 screws, with 2 mm silicon gaskets placed between the current collectors and the end plates, and the MEA placed between the flow-fields with the carbon gas diffusion layer (GDL). Gaskets punched from virgin silicon are used for sealing. In addition to electrical insulation, a relatively homogeneous compression can also be achieved by the silicon gaskets. The active area of the cell was machined to flow-fields with a single serpentine channel on titanium blocks. Both the width and depth of the channels are set to 1 mm, and the width of the lands is also 1 mm. Fig. 6b shows the actual picture of the PEM electrolyzer device.

Fig. 6c shows the poarization curves of the YZRO/AB and IrO_2/AB anodes of the PEM electrolyser at 25 °C. Obviously, the cell performance of the YZRO anode tested in the PEMWE is much higher than that of the commercial IrO_2 anode. At a voltage of 1.65 V, the current densities of the YZRO/AB electrolyser and the IrO_2/AB electrolyser are

0.34 A cm^{-2} and 0.18 A cm^{-2} at 25 °C, respectively, nearly 2-fold increase in current density for the YZRO/AB electrolyser than for the IrO_2 electrolyser, indicating a promising practical applications for YZRO/AB. Fig. 6d displays the EIS curves at a cell voltage of 1.55 V at 25 °C. As can be seen, the charge transfer resistance of the YZRO/AB electrolyser is smaller than that of the commercial IrO_2/AB electrolyser, consistent with the porlarization curve result.

4. Conclusion

For the first time, we developed the A site doped yttrium ruthenate pyrochlore, a highly active and stable OER electrocatalyst for water electrolysis in acidic media. By using the A site doping strategy in YRO, the prepared ruthenate pyrochlore achieved a much higher activity and stability in comparison with undoped YRO/AB and IrO_2/AB. The partial substitution of Y^{3+} by Zn^{2+} alters the electronic properties and the surface oxygen species, improving the electrical conductivity and providing more active sites for OER. Regarding the effect of the A-site cation of the ruthenate pyrochlore oxides on the catalysis towards OER, our findings suggest that the activity of these compounds would be further improved by carefully selecting the A- and B-site cations. The single cell test of the MEA with the YZRO/AB anode exhibits a higher performance compared to commercial IrO_2, indicating a promising practical applications for PEM water electrolysis. We believe that this work will provide new perspectives into the development of low cost OER electrocatalysts with high activity and acidic stability. The A site doped strategy may be also suitable for other ruthenate pyrochlore (A_2Ru_2O7) and iridate pyrochlore ($A_2Ir_2O_7$) which can promote the development of the OER electrocatalysts in PEM water electrolysis.

Acknowledgements

This work was financially supported by the Shenzhen Peacock Plan (KQTD2016022620054656), Shenzhen Key Laboratory project (ZDSYS201603311013489), Development and Reform Commission of Shenzhen Municipality 2017 (No. 1106), Guangdong Innovative and Entrepreneurial Research Team Program (2016ZT06N500), the National Key Research and Development Program of China (2017YFB0102701), and Development and Reform Commission of Shenzhen Municipality 2017 (No. 1181).

Appendix A. Supplementary data

Supplementary material related to this article can be found, in the online version, at doi:https://doi.org/10.1016/j.apcatb.2018.11.071.

References

[1] D. Lebedev, M. Povia, K. Waltar, P.M. Abdala, I.E. Castelli, E. Fabbri, M.V. Blanco, A. Fedorov, C. Copéret, N. Marzari, T.J. Schmidt, Chem. Mater. 29 (2017) 5182–5191.
[2] Q. Feng, X.Z. Yuan, G. Liu, B. Wei, Z. Zhang, H. Li, H. Wang, J. Power Sources 366 (2017) 33–55.
[3] S. Siracusano, N. Van Dijk, E. Payne-Johnson, V. Baglio, A.S. Aricò, Appl. Catal. B 164 (2015) 488–495.
[4] M. Carmo, D.L. Fritz, J. Mergel, D. Stolten, Int. J. Hydrogen Energy 38 (2013) 4901–4934.
[5] D. Galizzioli, F. Tantardini, S. Trasatti, J. Appl. Electrochem. 4 (1974) 57–67.
[6] K. Sardar, E. Petrucco, C.I. Hiley, J.D. Sharman, P.P. Wells, A.E. Russell, R.J. Kashtiban, J. Sloan, R.I. Walton, Angew. Chemie 53 (2014) 10960–10964.
[7] V.K. Puthiyapura, S. Pasupathi, H. Su, X. Liu, B. Pollet, K. Scott, Int. J. Hydrogen Energy 39 (2014) 1905–1913.
[8] X. Kong, K. Xu, C. Zhang, J. Dai, S. Norooz Oliaee, L. Li, X. Zeng, C. Wu, Z. Peng, ACS Catal. 6 (2016) 1487–1492.
[9] A.T. Marshall, S. Sunde, M. Tsypkin, R. Tunold, Int. J. Hydrogen Energy 32 (2007) 2320–2324.
[10] J. Cheng, H. Zhang, G. Chen, Y. Zhang, Electrochim. Acta 54 (2009) 6250–6256.
[11] M. Escudero-Escribano, A.F. Pedersen, E.A. Paoli, R. Frydendal, D. Friebel, P. Malacrida, J. Rossmeisl, I.E.L. Stephens, I. Chorkendorff, J. Phys. Chem. B 122 (2018) 947–955.
[12] E. Mayousse, F. Maillard, F. Fouda-Onana, O. Sicardy, N. Guillet, Int. J. Hydrogen Energy 36 (2011) 10474–10481.
[13] S. Siracusano, V. Baglio, S.A. Grigoriev, L. Merlo, V.N. Fateev, A.S. Aricò, J. Power Sources 366 (2017) 105–114.
[14] S. Siracusano, N. Hodnik, P. Jovanovic, F. Ruiz-Zepeda, M. Šala, V. Baglio, A.S. Aricò, Nano Energy 40 (2017) 618–632.
[15] R. Kötz, S. Stucki, Electrochim. Acta 31 (1986) 1311–1316.
[16] L. Wang, V.A. Saveleva, S. Zafeiratos, E.R. Savinova, P. Lettenmeier, P. Gazdzicki, A.S. Gago, K.A. Friedrich, Nano Energy 34 (2017) 385–391.
[17] X. Wu, K. Scott, Int. J. Hydrogen Energy 36 (2011) 5806–5810.
[18] K.S. Kadakia, P.H. Jampani, O.I. Velikokhatnyi, M.K. Datta, P. Patel, S.J. Chung, S.K. Park, J.A. Poston, A. Manivannan, P.N. Kumta, Mater. Sci. Eng. B 212 (2016) 101–108.
[19] J. Kim, P.C. Shih, K.C. Tsao, Y.T. Pan, X. Yin, C.J. Sun, H. Yang, J. Am. Chem. Soc. 139 (2017) 12076–12083.
[20] K. Sardar, S.C. Ball, J.D.B. Sharman, D. Thompsett, J.M. Fisher, R.A.P. Smith, P.K. Biswas, M.R. Lees, R.J. Kashtiban, J. Sloan, R.I. Walton, Chem. Mater. 24 (2012) 4192–4200.
[21] J. Park, M. Park, G. Nam, M.G. Kim, J. Cho, Nano Lett. 17 (2017) 3974–3981.
[22] J.B. Goodenough, R. Manoharan, M. Paranthaman, J. Am. Chem. Soc. 112 (1990) 2076–2082.
[23] K. Fujii, Y. Sato, S. Takase, Y. Shimizu, J. Electrochem. Soc. 162 (2014) F129–F135.
[24] G. Ehora, S. Daviero-Minaud, M.C. Steil, L. Gengembre, M. Frère, S. Bellayer, O. Mentré, Chem. Mater. 20 (2008) 7425–7433.
[25] C. Abate, V. Esposito, K. Duncan, J.C. Nino, D.M. Gattia, E.D. Wachsman, E. Traversa, J. Am. Ceram. Soc. (2010).
[26] J.-M. Bae, B.C.H. Steele, J. Electroceramics 3 (1999) 37–46.
[27] J.S. Lee, S.J. Moon, T.W. Noh, T. Takeda, R. Kanno, S. Yoshii, M. Sato, Phys. Rev. B 72 (2005) 035124.
[28] F. Ishii, T. Oguchi, J. Phys. Soc. Jpn. 69 (2000) 526–531.
[29] G. Berti, S. Sanna, R. Ruiz-Bustos, J. van Duijn, A. Brambilla, Á. Muñoz-Noval, F. Demartin, L. Duò, C. Castellano, RSC Adv. 5 (2015) 100809–100815.
[30] G. Berti, S. Sanna, C. Castellano, J. Van Duijn, R. Ruiz-Bustos, L. Bordonali, G. Bussetti, A. Calloni, F. Demartin, L. Duò, A. Brambilla, J. Phys. Chem. C 120 (2016) 11763–11768.
[31] H. Su, V. Linkov, B.J. Bladergroen, Int. J. Hydrogen Energy 38 (2013) 9601–9608.
[32] H. Su, B.J. Bladergroen, V. Linkov, S. Pasupathi, S. Ji, Int. J. Hydrogen Energy 36 (2011) 15081–15088.
[33] C. Rozain, E. Mayousse, N. Guillet, P. Millet, Appl. Catal. B 182 (2016) 153–160.
[34] Y. Liu, H. Dai, J. Deng, L. Zhang, Z. Zhao, X. Li, Y. Wang, S. Xie, H. Yang, G. Guo, Inorg. Chem. 52 (2013) 8665–8676.
[35] Y. Zhou, C.-K. Dong, L.L. Han, J. Yang, X.-W. Du, ACS Catal. 6 (2016) 6699–6703.
[36] H. Miao, Z. Wang, Q. Wang, S. Sun, Y. Xue, F. Wang, J. Zhao, Z. Liu, J. Yuan, Energy 154 (2018) 561–570.
[37] W. Sun, Y. Song, X.Q. Gong, L.M. Cao, J. Yang, ACS Appl. Mater. Interfaces 8 (2016) 820–826.
[38] B. Jian, Z. Xiaodong, F. Bo, Z. Jiajia, Z. Min, Y. Wenlong, H. Xin, W. Hui, P. Bicai, X. Yi, Angew. Chemie 127 (2015) 7507–7512.
[39] M. Pirzada, R.W. Grimes, J.F. Maguire, Solid State Ion. 161 (2003) 81–91.
[40] S. Yoshii, K. Murata, M. Sato, J. Phys. Chem. Solids 62 (2001) 129–134.
[41] A.S. Patra, G. Gogoi, R.K. Sahu, M. Qureshi, Phys. Chem. Chem. Phys. PCCP 19 (2017) 12167–12174.
[42] G.C. da Silva, N. Perini, E.A. Ticianelli, Appl. Catal. B 218 (2017) 287–297.
[43] J.-M. Hu, J.-Q. Zhang, C.-N. Cao, Int. J. Hydrogen Energy 29 (2004) 791–797.
[44] T. Reier, M. Oezaslan, P. Strasser, ACS Catal. 2 (2012) 1765–1772.
[45] J.O.M. Bockris, J. Chem. Phys. 24 (1956) 817–827.
[46] H. Over, Chem. Rev. 112 (2012) 3356–3426.
[47] J. Rossmeisl, A. Logadottir, J.K. Nørskov, Chem. Phys. 319 (2005) 178–184.
[48] S. Song, H. Zhang, X. Ma, Z. Shao, R.T. Baker, B. Yi, Int. J. Hydrogen Energy 33 (2008) 4955–4961.
[49] E. Rasten, G. Hagen, R. Tunold, Electrochim. Acta 48 (2003) 3945–3952.
[50] M.V. ten Kortenaar, J.F. Vente, D.J.W. Ijdo, S. Müller, R. Kötz, J. Power Sources 56 (1995) 51–60.
[51] T.R. Felthouse, P.B. Fraundorf, R.M. Friedman, C.L. Schosser, J. Catal. 127 (1991) 393–420.
[52] A.R. Hillman, M.A. Skopek, S.J. Gurman, Phys. Chem. Chem. Phys. 13 (2011) 5252–5263.
[53] S.C.H. G, N.M. Ling, K. Sarp, F. Daniel, O. Hirohito, N. Anders, Angew. Chemie 126 (2014) 7297–7300.